NASA Contractor Report 177971

NASA-CR-177971
19860001959

BRIDGMAN GROWTH OF SEMICONDUCTORS

Frederick M. Carlson

SCIENTIFIC CONCEPTS, INC.
Potsdam, New York

Contract NAS1-16721

National Aeronautics and
Space Administration

Langley Research Center
Hampton, Virginia 23665

1 Report No	2 Government Accession No	3 Recipient's Catalog No
NASA CR-177971		

4 Title and Subtitle	5 Report Date
Bridgman Growth of Semiconductors	September 1985
	6 Performing Organization Code

7 Author(s)	8 Performing Organization Report No
F. M. Carlson	
	10 Work Unit No

9 Performing Organization Name and Address	11 Contract or Grant No
Scientific Concepts, Inc. P.O. Box 5076, Pottsdam, NY 13676	NAS1-16721
	13 Type of Report and Period Covered
12 Sponsoring Agency Name and Address	Contractor Report
National Aeronautics and Space Administration Washington, DC 20546	14 Sponsoring Agency Code 694-80-70

15 Supplementary Notes

Langley Technical Monitor: A. L. Fripp

16 Abstract

The purpose of this study was to improve our understanding of the transport phenomena which occurs in the directional solidification of alloy semiconductors. In particular, emphasis was placed on the strong role of convection in the melt. Analytical solutions were not deemed possible for such an involved problem. Accordingly, a numerical model of the process was developed which simulated the transport. This translates into solving the partial differential equations of energy, mass, species, and momentum transfer subject to various boundary and initial conditions. A finite element method with simple elements was initially chosen. This simulation tool will enable the crystal grower to systematically identify and modify the important design factors within her control to produce better crystals.

17 Key Words (Suggested by Author(s))	18 Distribution Statement
Crystal Growth Directional Solidification Microgravity Fluid Flow	Unclassified - Unlimited Subject Category 34

19 Security Classif (of this report)	20 Security Classif (of this page)	21 No of Pages	22 Price
Unclassified	Unclassified	33	A03

For sale by the National Technical Information Service Springfield Virginia 22161

CONTENTS

1.0 INTRODUCTION

1.1 OVERVIEW

The Bridgman method has been employed over the years to grow crystals of many different materials. The desired result is usually a large single crystal having uniform properties. When the Bridgman technique is used to grow semiconductor materials crystal defects including dislocations, twins, compositional inhomogeneities, and cracking are encountered at an increasing rate as crystal diameter increases. These problems are believed to be caused by convection which originates from the interaction between the spatially dependent density field and the local gravitational field. Since in most instances little can be done about the density variations, growers sought to reduce the level of convection by resorting to space processing. The results of these early experiments brought to light how meager was our understanding of the transport phemonena involved in the growth process. Additional problems experimentalists have grappled with which complicate the process involve the high temperature levels, opacity of the fluid, and complexity of the physics. What is needed is a deeper understanding of the heat and mass transport which occurs during the growth process. Convection is not inherently bad. It may be very useful if it can be controlled. This control will enable the crystal grower to produce larger diameter single crystals.

The purpose of this study was to improve our understanding of the transport phenomena which occurs in the directional solidification of alloy semiconductors. In particular, emphasis was placed on the strong role of convection in the melt. Analytical solutions were not deemed possible for such an involved problem. Accordingly, a numerical model of the process was developed which simulated the transport. This translates into solving the partial differential equations of energy, mass, species, and momentum transfer subject to various boundary and initial conditions. A finite element method with simple elements was initially chosen. This simulation tool will enable the crystal grower to systematically identify and modify the important design factors within her control to produce better crystals. The remainder of this report will outline the procedure and present the primary results.

1.2 MATHEMATICAL DESCRIPTION

A mathematical model of the transport of mass, energy, species, and momentum, that adequately describes the growth of typical semiconductor compounds is developed below. The geometric configuration is that of the vertical Bridgman technique as depicted in figure 1. Only vertical axisymmetric conditions are considered although this is not a limitation of the method.

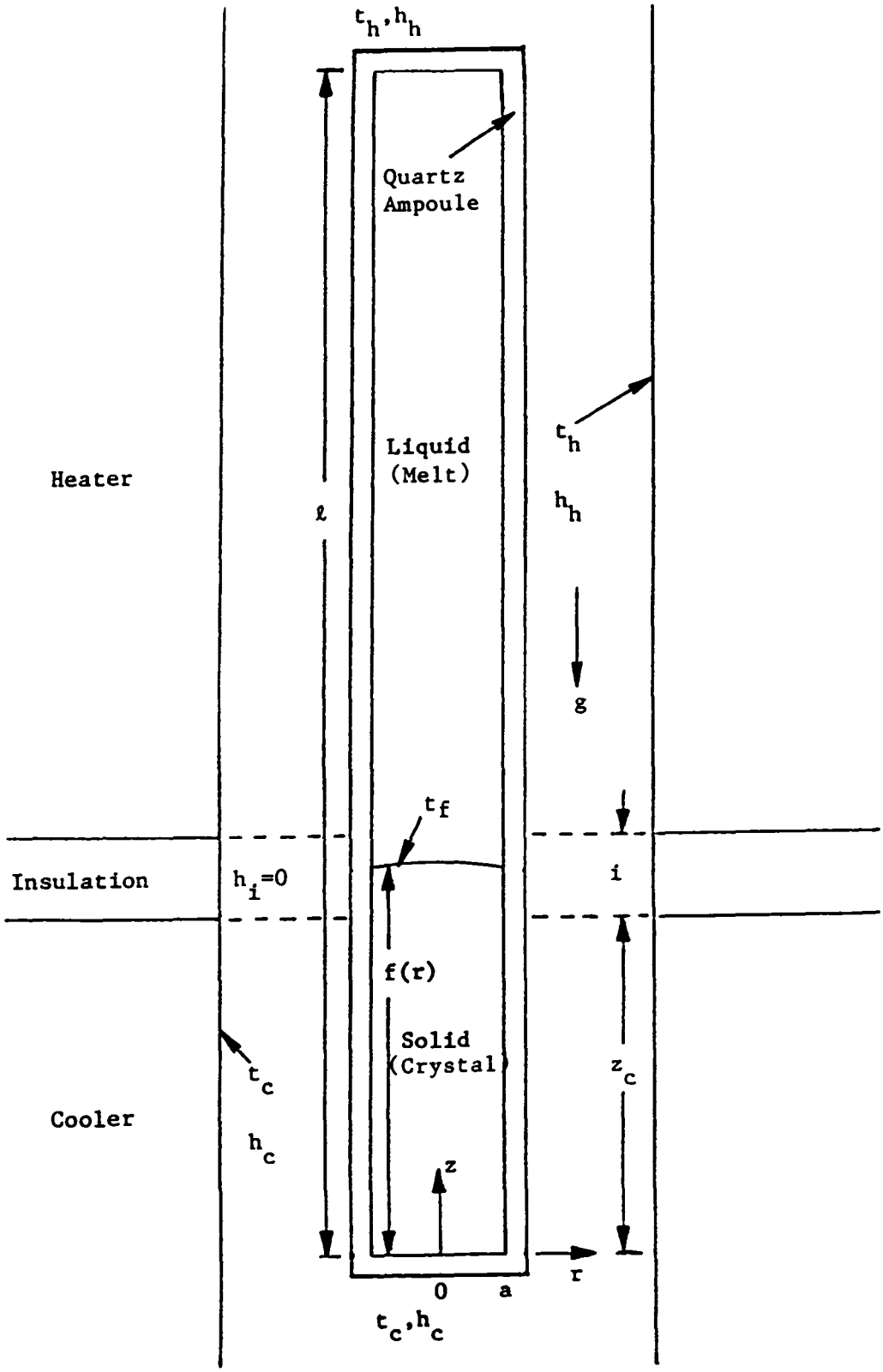

Figure 1. Bridgman Crystal Growth

The form of all the governing partial differential equations is:

$$\left[\frac{\partial}{\partial\tau}(\Gamma\phi) + \nabla\cdot(\Gamma\phi\vec{U})\right] + \frac{\partial\phi}{\partial\tau} + \nabla\cdot(\phi\vec{U}) = \nabla\cdot(\frac{\delta}{\rho_o}\nabla\phi) + \frac{\sigma}{\rho_o}$$

———— BOUSSINESQ ————

———————— EXACT ————————

where

$$\rho = \rho_o + \rho'(\vec{x},\tau) = \text{density}$$

$$\Gamma = \rho'/\rho_o$$

Table 1. gives the value of the dependent variable for each of the conservation equations. Only the two dimensional form is shown.

VARIABLE	MASS	ENERGY	SPECIES	R-MOMENTUM	Z-MOMENTUM
ϕ	1	$C_p T$	c	U	W
δ	0	k/C_p	D	μ	μ
σ	0	0	0	$-\frac{\partial P}{\partial R}$	$-\frac{\partial P}{\partial Z} + \rho g_z$

Table 1. Conservation equation dependent variables.

The boundary conditions include:

Walls:

$-k(dt/dn) = h(t-t_\infty)$, convection heat transfer,
$dc/dn = 0$, zero mass transfer,
$U = 0$, no slip condition.

Interfacial:

$t_l = t_s = t_f$, equal temperature,

$k(dt/dn)_s - k(dt/dn)_l = 0$, zero growth energy balance,

$D(dc/dn) = V_f(K-1)c$, mass balance.

While these boundary conditions are not necessarily the most general form they include all the cases of interest. When the differential equations and boundary conditions are nondimensionalized the following groups of parameters appear:

$Bi = ha/k$, Biot number,

$\gamma = 2x_0V_f/D$, growth rate,

$\eta = (f(a) - f(0))/a$, interface curvature index,

$Pr = \mu C_p/k$, Prandtl number,

$Gr = g\beta\Delta Ta^3(\rho_0/\mu)^2$ thermal Grashof number,

$Sc = \mu/(\rho D)$, Schmidt number.

Only the parameters which will be discussed in the text have been included. The subject of initial conditions will be deferred to a later section.

Little numerical work had been done on this set of equations for crystal growth problems when the project began. It was therefore necessary to develop a model to simulate the process and few examples were available. Consequently, a model was developed and validated by combining information from many simple, abridged cases. The following sections will outline these cases, discuss the relevance of the results, and show how they contributed to the state of the art as it exists today.

2.0 CONDUCTION HEAT TRANSFER

Solidification is a process primarily controlled by heat transfer. Initial effort was directed at developing a model which would predict the location of the solid-liquid interface during steady state operation when the ampoule was stationary. It is well known from experiments that interface shape and location strongly influence crystal quality. Only conduction effects were included with other effects added later as development progressed.

The model is for axisymmetric conditions with the gravitational vector aligned with the negative axial direction and the melt on top. Additional assumptions made were:

(i) all material properties are constant,
(ii) the ampoule walls are of zero thickness and hence are excluded from the heat transfer analysis,
(iii) the furnace temperature is uniform in each section,
(iv) heat exchange between the ampoule and the furnace can be represented by a constant, but different, heat transfer coefficient in the heater, adiabatic zone, and the cooler.

Since the computational domain includes a curved boundary, (the solid-liquid interface), a finite element technique was used to construct a numerical solution. This was chosen because finite difference methods with a grid that follows coordinate surfaces were felt to be too difficult to use. Galerkin's method and a computational mesh of linear triangular elements were used to discretize the differential equation which was solved using a modified Gauss-Siedel method.

The governing equation and boundary conditions provide the key to which potential parameters might influence interface curvature and location. These parameters include heater and cooler Biot numbers, solid-liquid thermal conductivity ratio, dimensionless interface temperature, insulation zone thickness, and ampoule location within the furnace. Numerical experiments were conducted, the results of which are presented below. The process is sufficiently complex such that a general correlation of these parameters could not be found.

The parameters which strongly influence the interface are Biot number, conductivity ratio, dimensionless interface temperature, and ampoule axial location within the furnace. Some of the results are presented in figures 2 through 4. Ampoule end effects become important when the interface is within a few ampoule diameters of either end. Influence of axial location, when end effects are excluded, can be minimized by proper choice of the temperature boundary conditions. Insulation zone thickness was not critical and is omitted here. A detailed account can be found in [1].

The interface curvature index η is a measure of the degree of curvature of the interface. A planar interface has a zero index. Illustrated in Figure 2a is a plot of η versus the dimensionless interface temperature for various conductivity ratios and Biot numbers. Values of insulation zone thickness ($I = 1$) and zone location within the furnace ($Z_c = 17.5$) are held constant. At this value of Z_c the center of the ampoule coincides with the center of the insulation zone and end effects may be

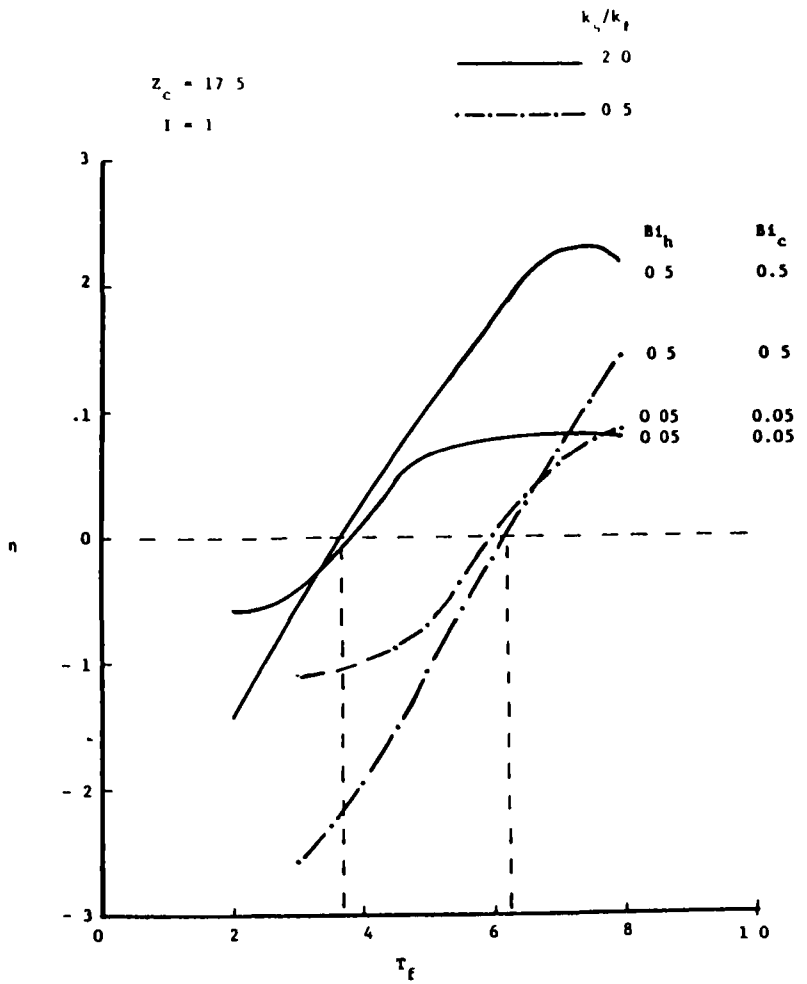

Figure 2a. Dimensionless interface curvature versus temperature.

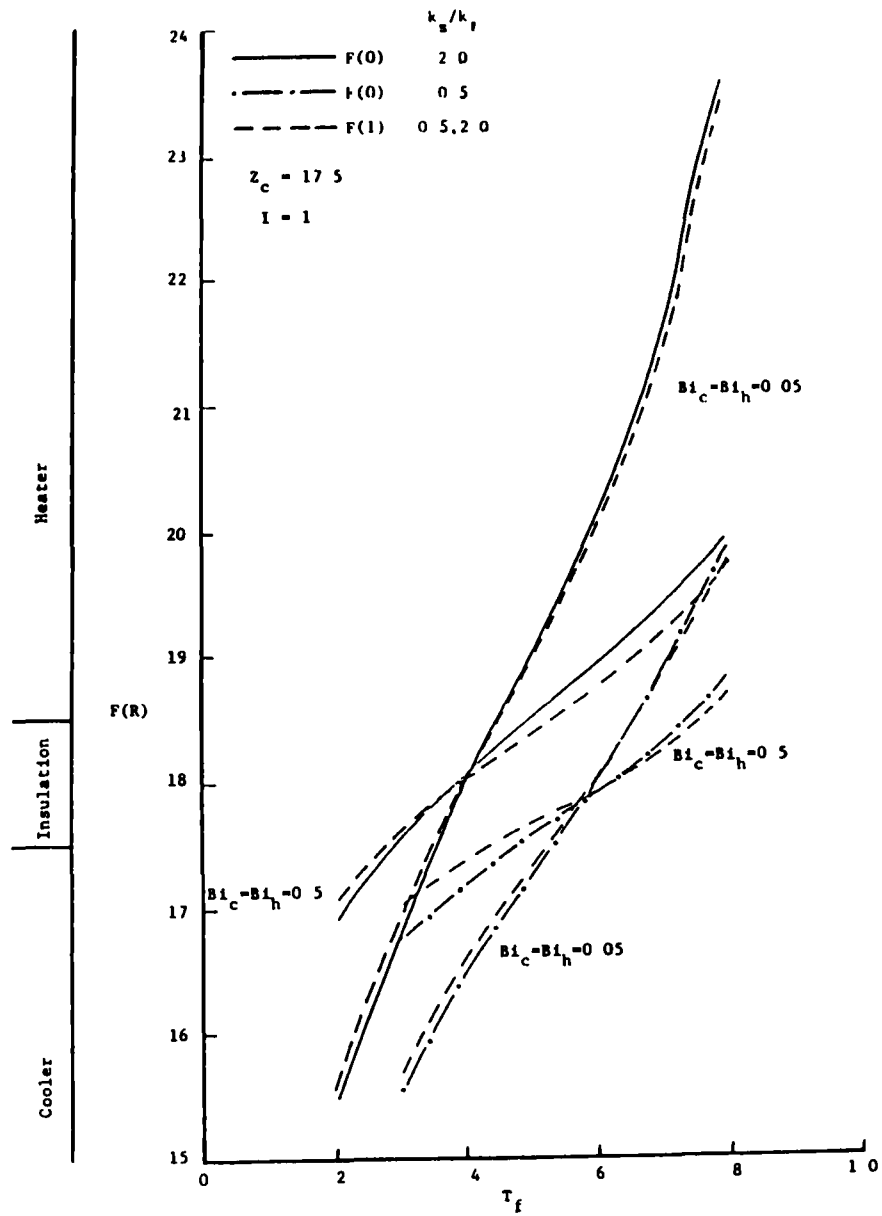

Figure 2b. Dimensionless interface position versus temperature.

safely ignored. Study of this figure reveals that η is very sensitive to conductivity ratio k_s/k_l. This fact makes accurate knowledge of this material property requisite to prediction of interfacial curvature and position. It can also be seen that η is sensitive to T_f. While material properties for a given system are fixed, T_f is not, and thus the crystal grower has a measure of control in adjusting the interface during the process. Exactly how one accomplishes this is no simple matter and must be analyzed on a case by case basis.

A plot of dimensionless interface location at the centerline and at the ampoule wall is shown in figure 2b as a function of T_f. The above T_f and k_s/k_l sensitivity can be seen in this figure along with how the zero curvature index location varies with axial location within the furnace. All planar interfaces are located within the insulated zone. This is not surprising since the heat transfer is primarily axial in this region and hence isotherms, (the interface is an isotherm), are nearly axial planes. It should also be noted that as Biot number approachs zero the curvature index also goes to zero. Physically, the Biot number is the ratio of the resistance to heat transfer within the material to that between the furnace and the material. Small Biot numbers thus imply small internal radial temperature gradients with corresponding small interface curvatures. The effect of Biot number on η is large when T_f is in a range such that η is large. If T_f is adjusted to produce a small η, then the Biot number sensitivity decreases to a point where it is no longer an important parameter. This occurs at $T_f = 0.37$ and 0.625 for $k_s/k_l = 2.0$ and 0.5, respectively, in this figure.

Variations in T_f and k_s/k_l strongly influence η as can be seen in figure 3a where curvature is plotted as a function of heater Biot number. When Bi_h is greater than one the effect is small. This allows the crystal grower to set a T_f which will result in a planar interface. As Bi_h approaches zero all η tend toward zero for a wide range of T_f. Figure 3b confirms this fact and also illustrates how nearly planar interfaces are located within the insulation zone. Similar results occur as the cooler Biot number is varied.

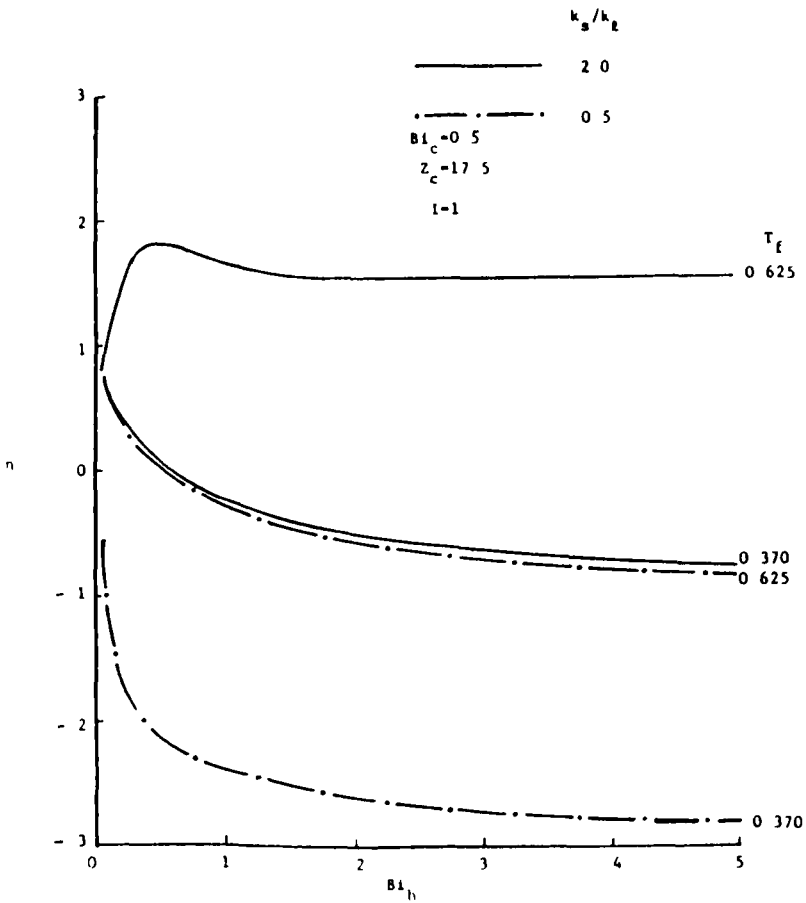

Figure 3a. Dimensionless interface curvature versus heater Biot number.

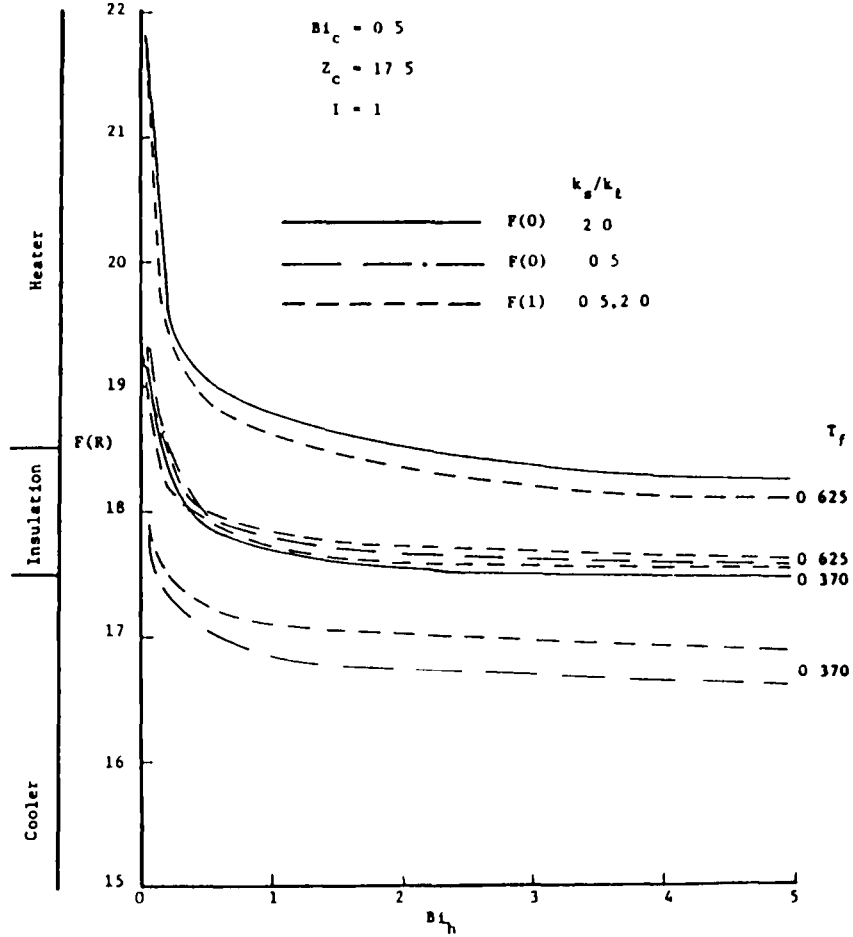

Figure 3b. Dimensionless interface position versus heater Biot number.

Discussion thus far has focused on a system which is centered within the furnace. During the initial and final stages end effects become important as figure 4 illustrates. At low ampoule withdrawal rates the transient effect will be minimal and η can be controlled by appropriately varying T_f. Since t_f is fixed, this can be accomplished by varying t_h or t_c. When the ampoule is at an intermediate axial position a nearly constant T_f can be chosen to yield a planar interface. It should be noted that there are cases where ''end effects'' persist for all ampoule locations (e.g., $T_f = 0.625$, $k_s/k_l = 2$).

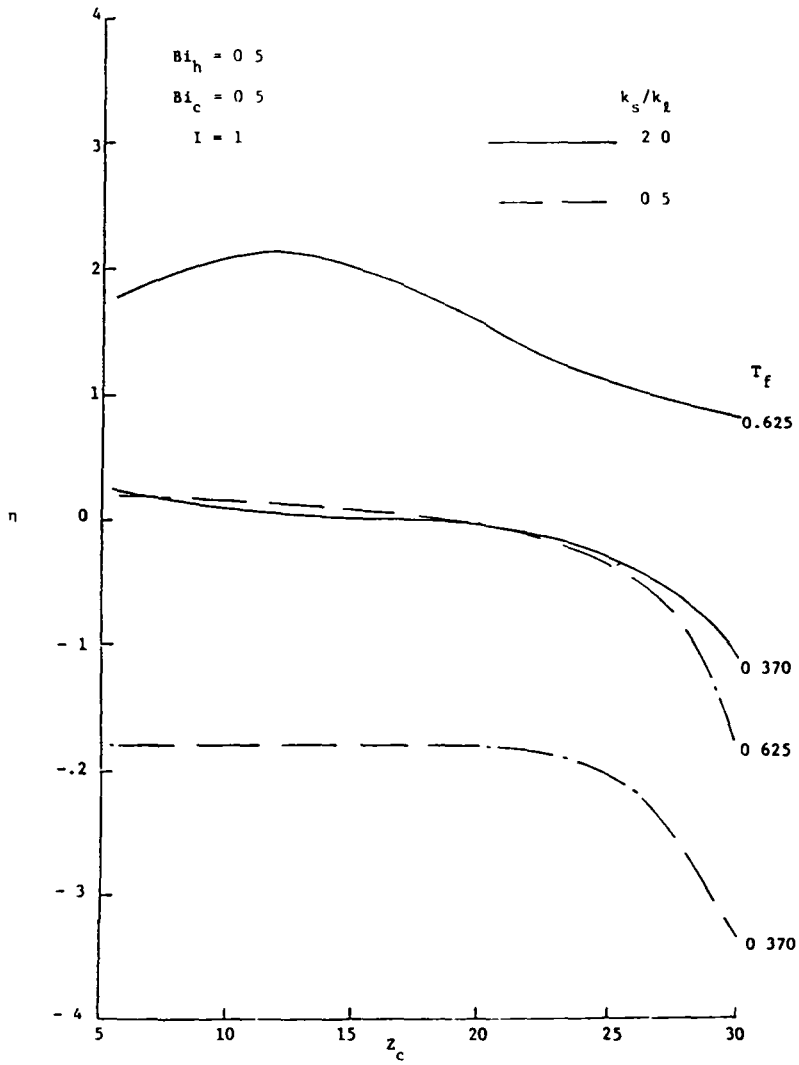

Figure 4. Dimensionless interface curvature versus ampoule adiabatic zone position.

In conclusion, numerical experiments show interfacial curvature is strongly influenced by charge solid-liquid thermal conductivity ratio, dimensionless interface temperature ratio, ampoule position, furnace Biot numbers and to a much lesser extent by insulation zone thickness. Consequently, the material properties must be accurately known if any prediction scheme is to yield meaningful results. It has also been demonstrated that curvature can be made independent of Biot number and ampoule position if the dimensionless interface temperature is properly chosen. Dimensionless interface temperature ratio thus becomes the dominant controlling parameter available to the crystal grower for achieving a particular interface shape. This is a significant result.

3.0 DIFFUSION CONTROLLED MASS TRANSFER

The macroscopic interface shape strongly influences the lateral solute segregation during unidirectional solidification. Since the interface is largely determined by heat transfer in dilute mixtures, a diffusion controlled mass transfer model was developed. The species transport equation has a form which is similar to the energy transport equation. The primary difference lies in the boundary conditions. Therefore, solution to the mass transport problem will increase confidence in the heat transfer solution of the previous section and add a new set of boundary conditions to our arsenal.

Steady state mass transfer in a two-dimensional cartesian system was studied because some limited analytical solutions were available to compare the results. A schematic diagram of the process is shown in figure 5. The interface shape was specified as parabolic. This was chosen because solutions from the heat conduction model predicted similar shapes.

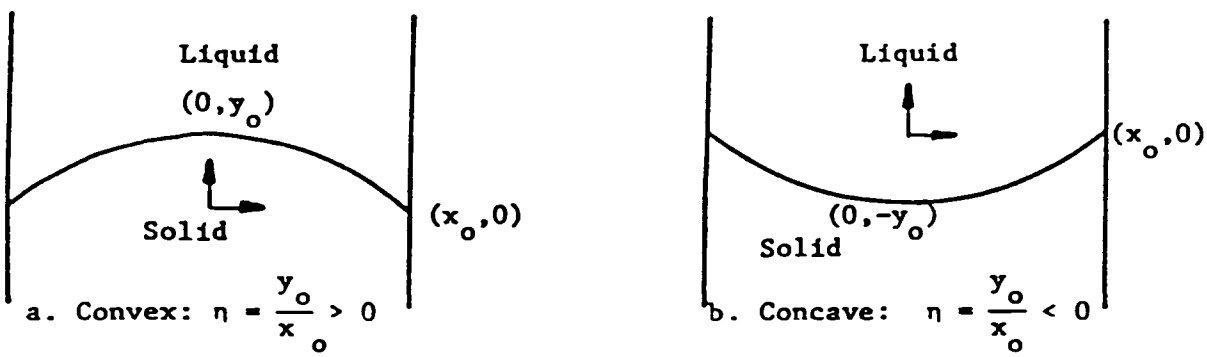

Figure 5. Geometry and coordinate system for unidirectional solidification with a non-planar solid liquid interface.

The key dimensionless parameters investigated were the non-planar interface shape, ($\eta = y_0/x_0$), the distribution coefficient, (K), and the combined effect of the diffusivity, growth speed, and container width ($\gamma = 2x_0 V_{f/D}$). The model was compared to an exact solution for a planar interface and an approximate analytical solution for a slightly curved interface. The agreement was excellent [2].

The influence of non-planar interface shape on lateral solute segregation is presented in figure 6 in terms of the interface concentration in the solid at the center and at the container wall, i.e., $C_s(0)$ and $C_s(1)$, as a function of η for K= 0.1. For any η, the vertical distance between solid and dotted lines at the same γ represents the solute concentration difference between the wall and the centerline. Figures for other K values all show a similar trend, namely, the larger the absolute value of η, the larger the concentration difference across the container for constant γ. This result demonstrates the expected trend that lateral solute segregation increases with increasing interface curvature. For $K < 1$, i.e., solute rejected from the solid phase to the liquid phase, the concentration at the wall is always higher than at the center for a convex interface and lower for a concave interface. This phenomenon is reversed for $K > 1$.

In figure 7 solute segregation is plotted as a function of η for various K's at $\gamma = 20.0$. This plot indicates that segregation is not linearly dependent on η except as $\eta \rightarrow 0$ as predicted by linear theory. For any non-planar shape, segregation is significantly enhanced as K deviates from unity.

The effect of the parameter γ on lateral segregation for fixed interface curvature is shown in figure 8. The numerical results clearly suggest the existance of a segregation maxima. At values of K far from unity, a maximum is clearly evident and becomes less obvious as K approaches 1. The dashed curves in figure 8 represent the maximum loci with K as an implicit parameter for convex and concave interfaces. Both cases indicate that the value of γ_{max}, which corresponds to the maximum segregation, decreases with increasing K for a fixed interface shape. Therefore, for the same curvature, the maximum segregation will occur at higher growth speeds for systems with smaller distribution coefficients. This figure also shows that as γ approaches zero or becomes very large, the degree of segregation decreases sharply.

It is of some interest to examine how η, γ, and K affect the

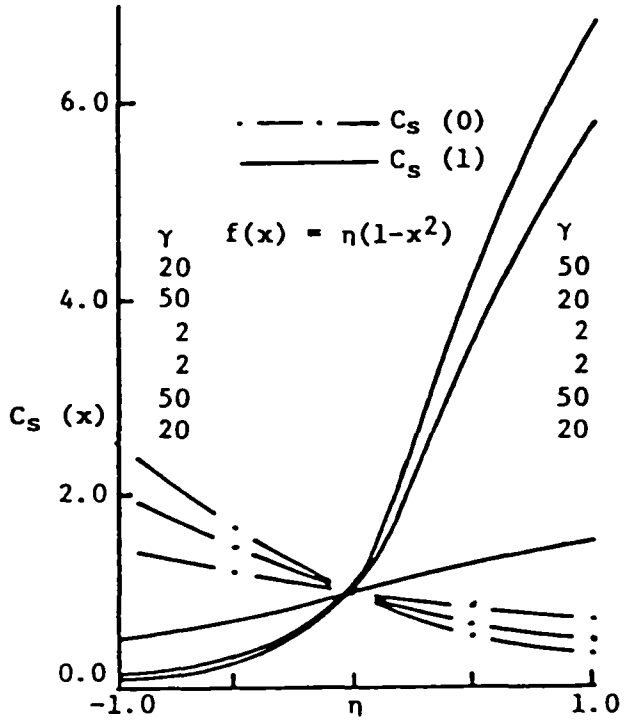

Figure 6. Solid interface concentration at the center and at the ampoule wall versus curvature index for K = 0.1 and γ=2, 20, 50.

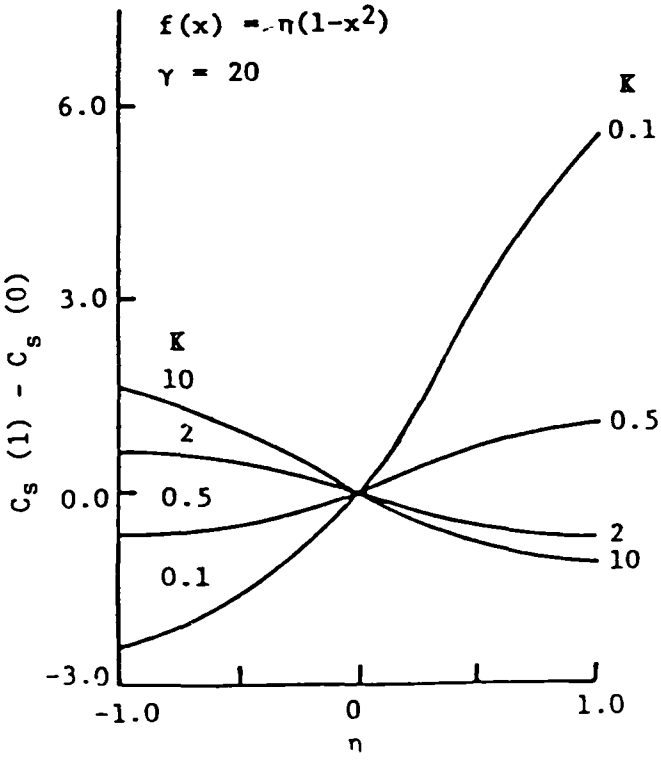

Figure 7. Lateral solute segregation versus curvature index for γ = 20 and K= 0.1, 0.5, 2.0, 10.0.

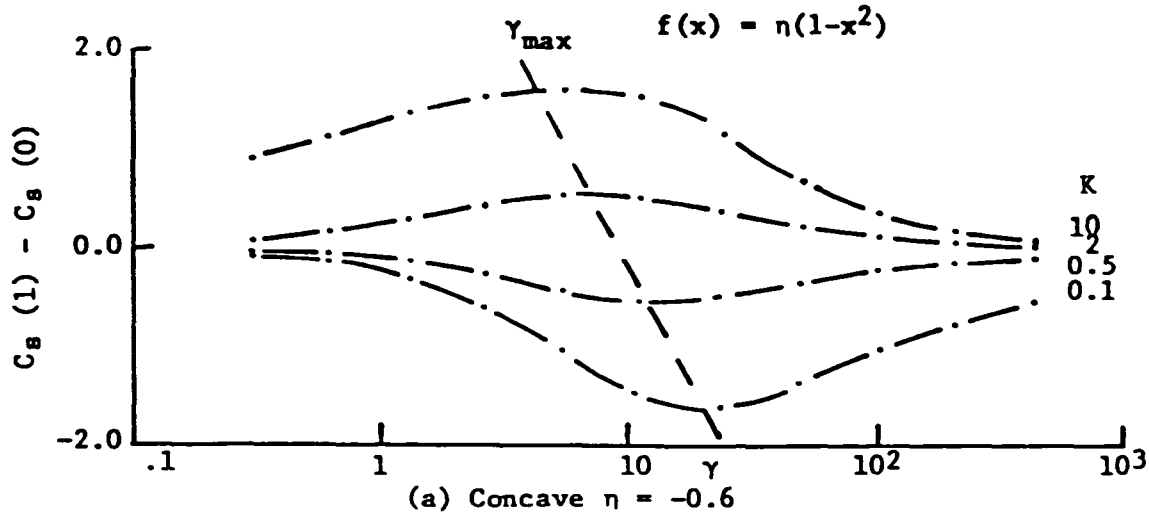

(a) Concave $\eta = -0.6$

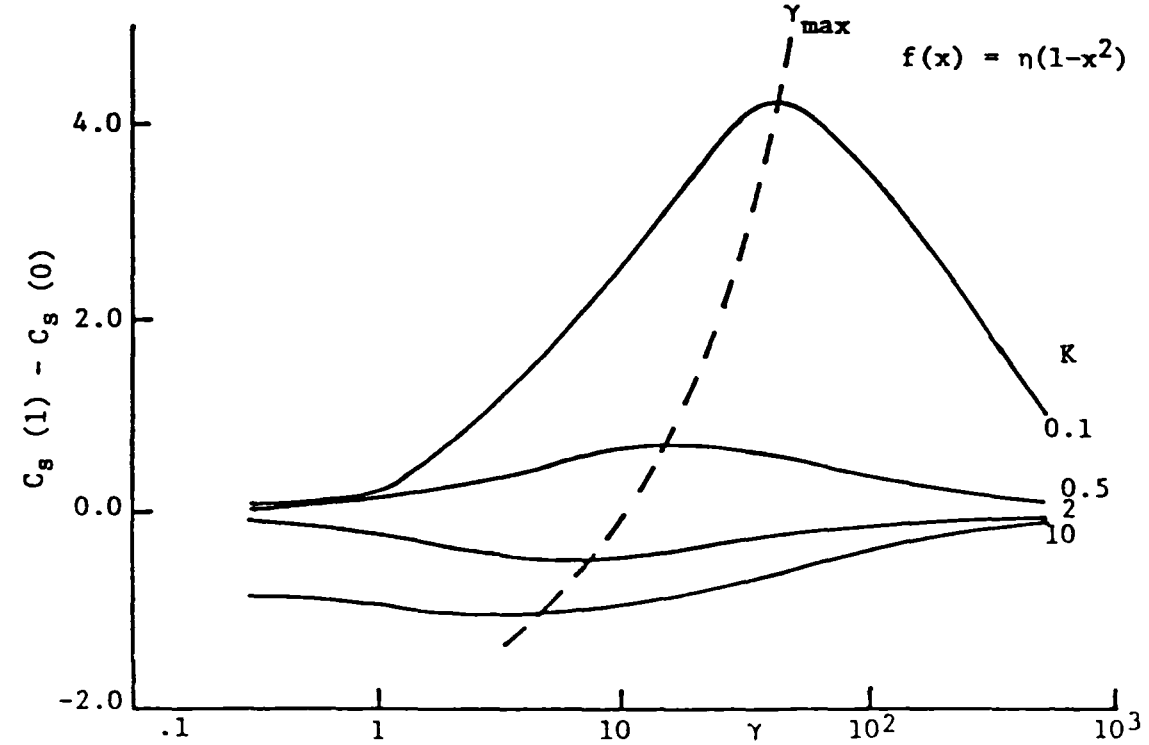

(b) Convex $\eta = 0.6$

Figure 8. Dependence of lateral solute segregation on the parameter η for K = 0.1, 0.5, 2, 10.

concentration profile in the solid. In figure 9 the concentration profiles for K = 0.5 and γ= 20.0 are compared for several values of η. For all cases with convex interfaces the profiles are similar in shape becoming flat for x < 0.7 and increasing

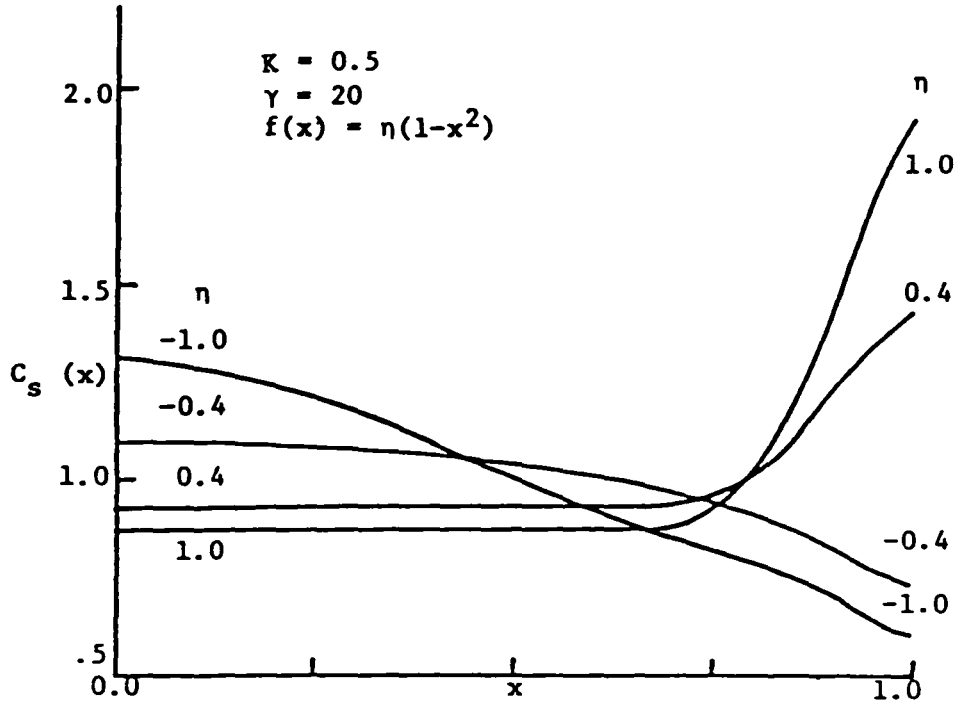

Figure 9. Solid lateral interface concentration for various values of interface curvature index.

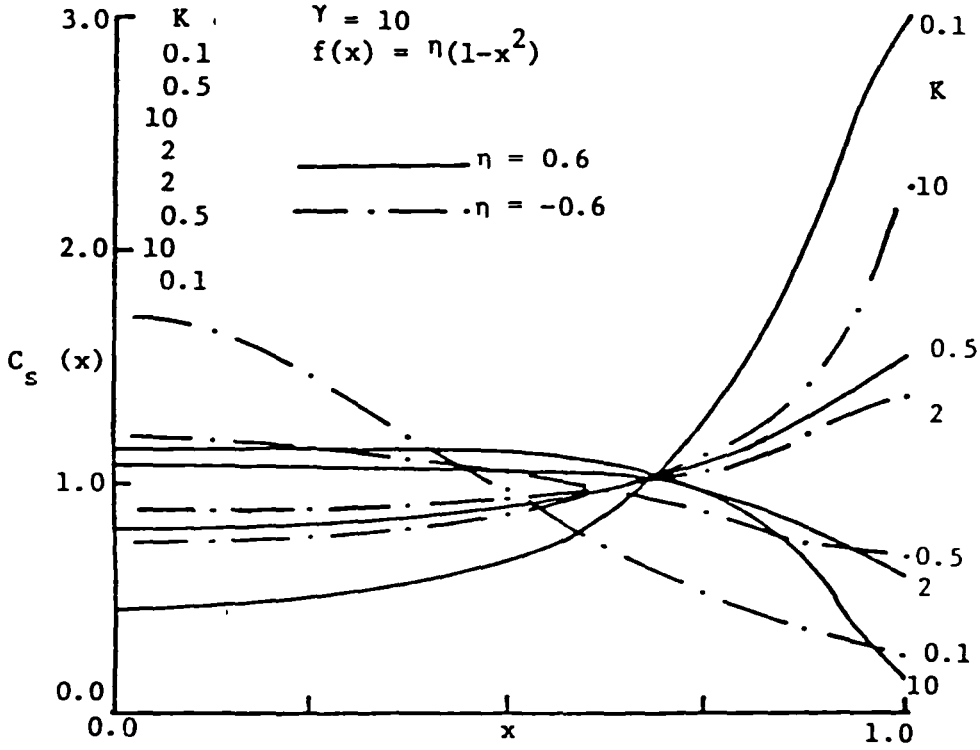

Figure 10. Solid lateral interface concentration for various values of distribution coefficient.

dramatically in the region near the wall. Similarly, for cases with concave interfaces concentration profiles are independent of location in the central region of the container and change appreciably near the wall. For $\eta < -0.6$, the concentration profile is strongly dependent on location throughout the container.

Figure 10 illustrates the dependence of the solute distribution along the interface on K. When comparing K = 0.1 through K = 10.0 for all curvatures it again can be seen that the segregation profile is relatively flat in the central region and rapidly changes in the vicinity of the wall with the effect becoming more pronounced as K deviates from unity. When K is far from unity the profile becomes a strong function of location.

The final point to be made in this section is shown graphically in figure 11. The segregation profile is found to be relatively flat for $x < 0.7$ for all values of γ. It appears that this parameter only influences the profile in the vicinity of the wall and its influence becomes greater as its magnitude increases.

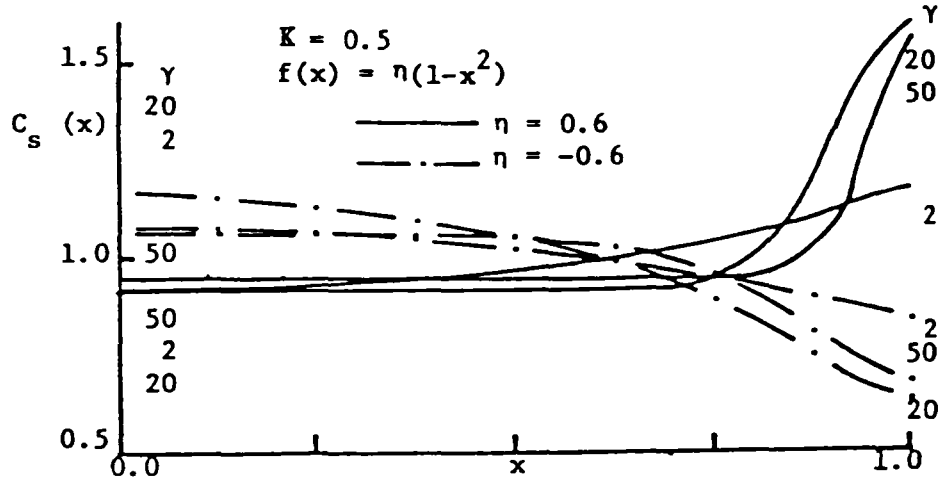

Figure 11. Influence of parameter γ on the interface concentration profile in the solid.

4.0 CONVECTION

Free convection is induced by density differences in the presence of a gravitational field. The interface temperature varies with concentration and the density is a function of both temperature and concentration in multicomponent melts. Motion arising from temperature and compositional variations (thermosolutal convection) requires the simultaneous solution of five partial differential equations for a laminar two-dimensional system. This section will address various subsets of the general

transient convection problem.

4.1 STEADY STATE THERMAL CONVECTION

This section is restricted to the study of a single component melt in which density depends solely on temperature. Steady state conditions prevail. In an effort to save computational time only the melt region is studied. It has been assumed that conditions in the crystal are such that the interface shape and location are known even though it could be calculated by the methods of section 1. Discussion centers on a melt contained within a vertical ampoule which is heated along its upper portion and cooled along the bottom portion. These portions are separated by an adiabatic zone which has an axial length of one ampoule radius. The bottom corresponds to the solid-liquid interface which is an isotherm and parabolic in shape. A paper [3] contains the details of numerical experiments which study the influence of various parameters on the flow characteristics. The important highlights will be presented here.

In the paper the governing equations were manipulated and it was clearly shown that radial temperature gradients drive the flow in the presence of an axial gravitational field. Flow persists as long as the gravitational field and the density (temperature) gradient are not everywhere in the same direction. There is no ''threshold'' Grashof number in this ''thermally stable'' configuration.

Probably the most interesting parameter is that of interface curvature index η. Interface curvature is a function of the heat flow path lines which at all points are normal to isothermal lines when convection is absent. Heat is coming into the ampoule from the top heater and leaving the bottom heater. The axial position where the isotherm curvature changes from convex (toward the hot end) to concave (toward the cold end) is the position where the radial gradient changes its sign. If this position occurs in the liquid (as indicated by a concave interface) then the radial temperature gradient which is the driving force for convection changes sign and two or more cells are formed. As η becomes more negative a lower cell is initiated near the centerline of the ampoule and proceeds to grow toward the wall while the upper cell becomes progressively weaker (Figure 12). It should be noted that while each cell is well mixed, mass transfer between cells is only by diffusion. When the interface is convex, a single counterclockwise cell occupies the entire region. In this configuration, maximum cell velocity increases as curvature index becomes more pronounced, resulting in greater overall mixing. These results also show that the flow cannot be characterized solely by Grashof number.

Increasing the insulation zone thickness would tend to decrease the absolute value of the interface index in actual

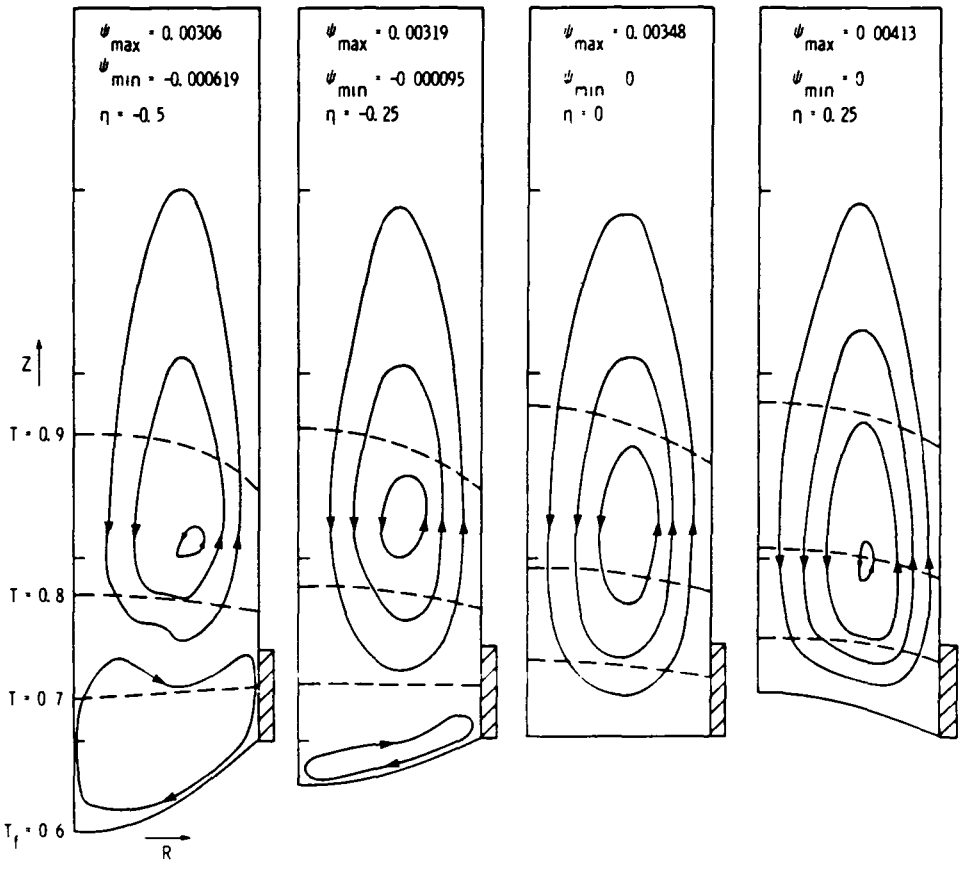

Figure 12. Streamlines and isotherms for various η when Bi = 0.5, Gr = 10,000, I = 0.5, Pr = 0.1.

crystal growth situations. This is done at the expense of decreasing the interfacial normal temperature gradient which may lead to problems with constitutional supercooling. If curvature index is negative and the insulation zone becomes thicker, then the top cell mixing decreases and its center of rotation moves upward along the ampoule wall as can be seen in figure 13. Simultaneously the bottom cell increases its mixing. The single cell convex interface case behaves the same as the top cell in the concave case. Changing the insulation zone thickness modifies the radial temperature gradient which drives the convection.

Increasing the Grashof number augments the overall level of mixing. Figure 14 shows that when two cells are present, the lower one is always more sensitive to changes in Grashof number than the upper one. A change in Grashof number by a factor of four doubles the cell characteristic velocity. When this large increase is due to changes in gravitational intensity, virtually no change can be observed in the temperature field.

The Biot number is the dimensionless ratio of internal to external heat flow resistance, i.e., how easily heat flows by

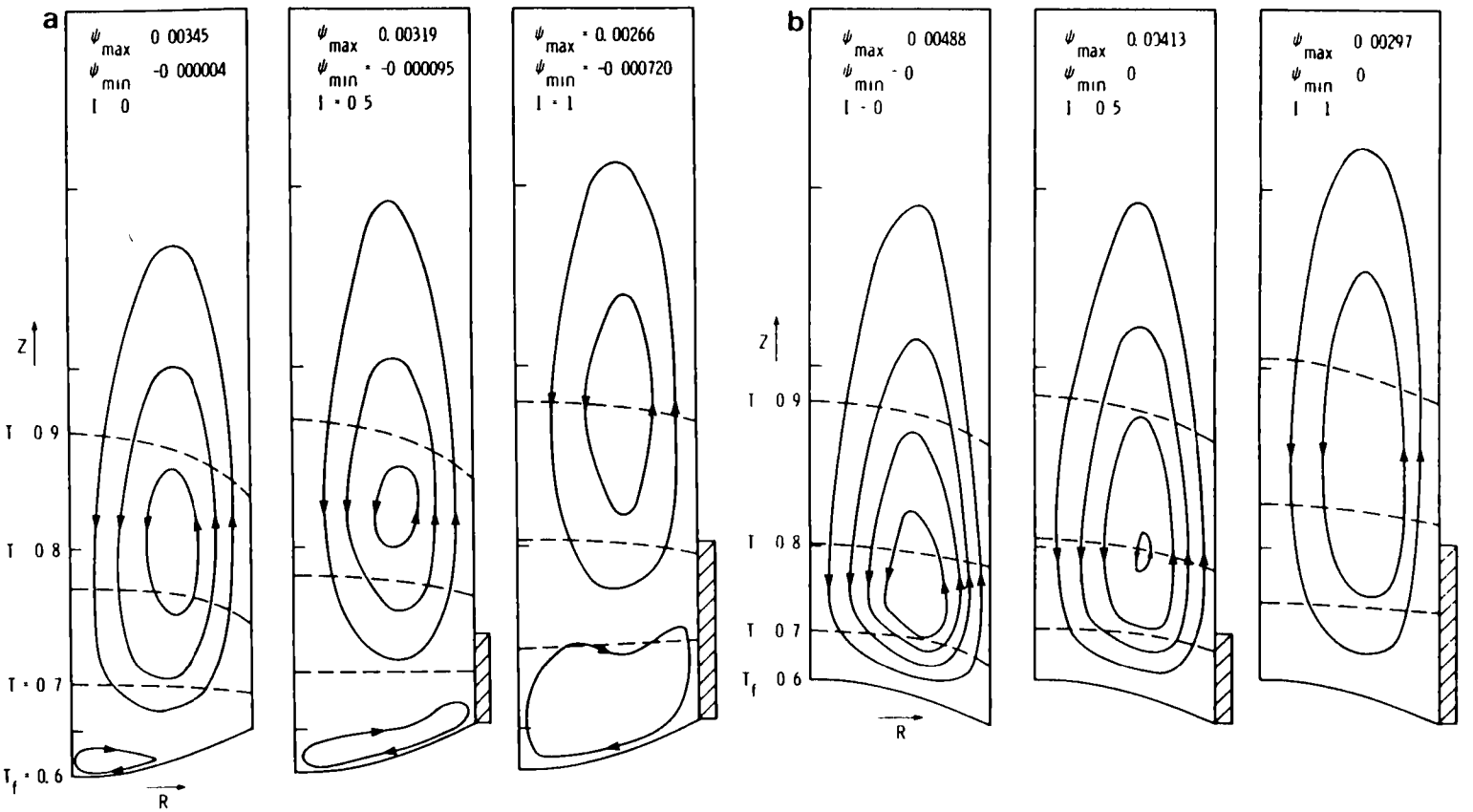

Figure 13. Streamlines and isotherms for (a) $\eta = -0.25$ and (b) $\eta = 0.25$ for various I when Bi = 0.5, Gr = 10,000, Pr = 0.1.

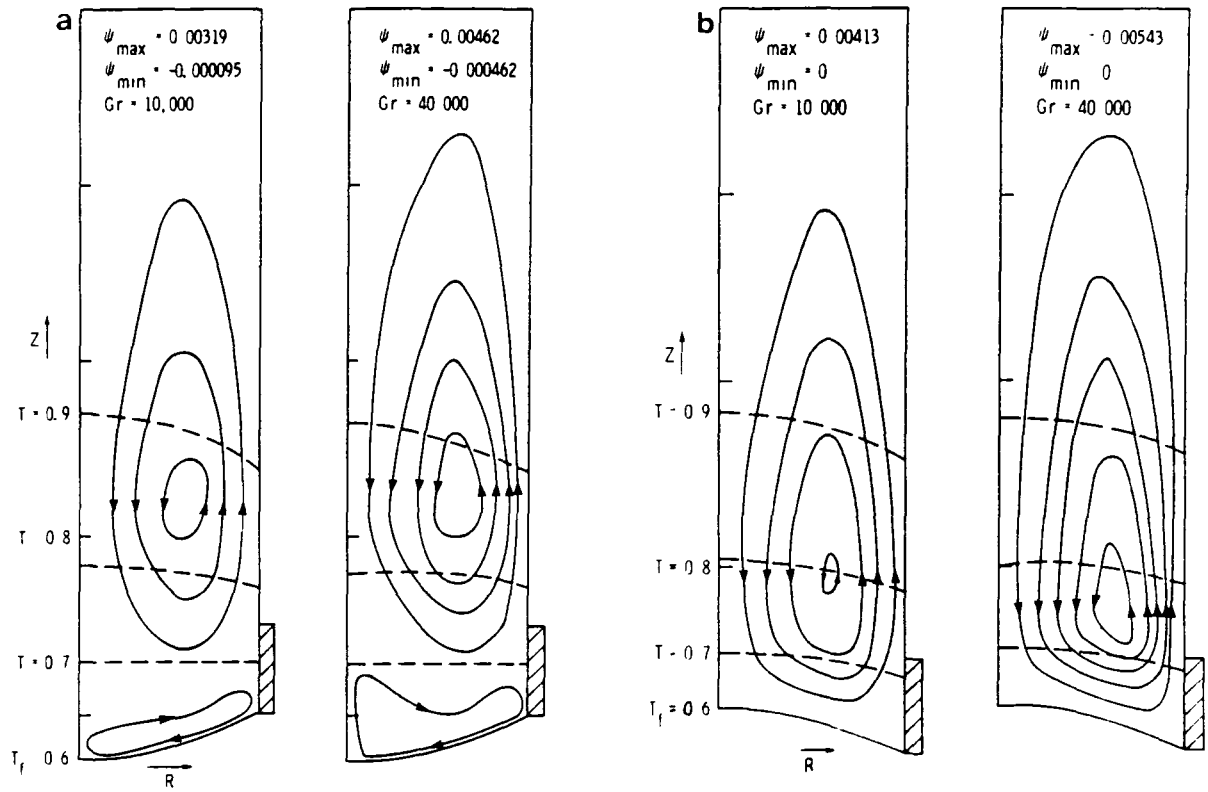

Figure 14. Streamlines and isotherms for (a)η = -0.25 and (b)η = 0.25 for various Gr when Bi = 0.5, I = 0.5, Pr = 0.1.

conduction within the ampoule to how easily heat is transferred to the ampoule wall from the heater. A small Biot number implies a small internal resistance to heat flow compared to the external resistance. A more uniform melt temperature is expected for small Bi, which should result in smaller radial temperature gradients and less convection. Data in figure 15 exhibit these trends for both single and multiple cell fields.

The flow field is governed by the conservation partial differential equations in conjunction with the boundary conditions and by the flow parameters within the equations such as Grashof and Prandtl number. The boundary condition which predominates in the upper region is the wall Biot number. In the lower cell the specified interfacial temperature and shape dominate. It is interesting that in the lower region, greater mixing results as Bi decreases. This is opposite to the trend in the upper region.

While the Biot number influences the flow and thermal fields through the boundary conditions, the Prandtl number makes its presence felt through the energy equation. There, it amplifies

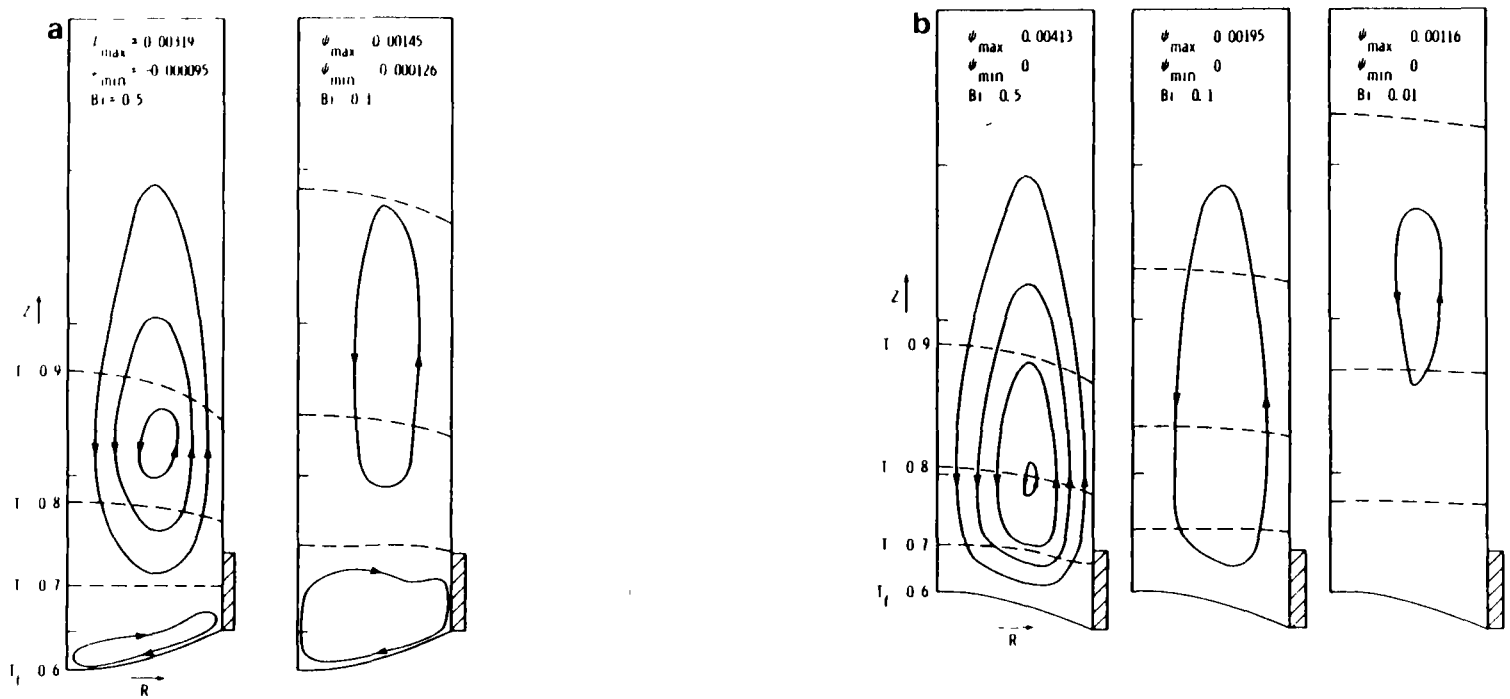

Figure 15. Streamlines and isotherms for (a) η = -0.25 and (b) η = 0.25 for various Bi when Pr = 0.1, Gr = 10,000, I = 0.5.

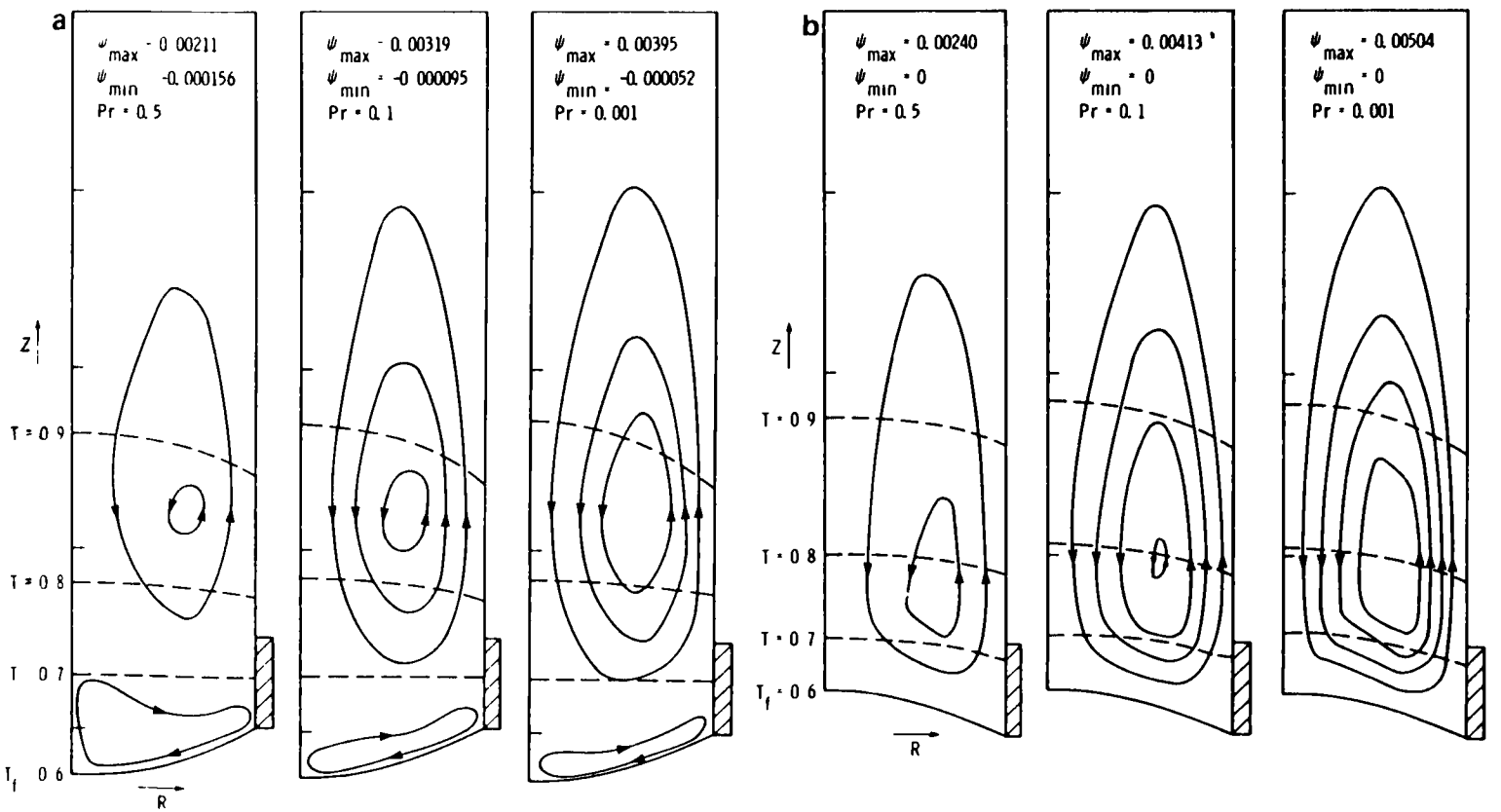

Figure 16. Streamlines and isotherms for (a) $\eta = -0.25$ and (b) $\eta = 0.25$ for various Pr when Bi = 0.5, Gr = 10,000, I = 0.5.

the influence of the convective terms on the temperature field. As Pr decreases, convection should have less influence on the temperature field. Thus, larger temperature gradients and larger velocities are expected in lower Pr fluids. Figure 16 confirms this reasoning for the upper cell. The lower cell again exhibits the opposite trend, just as for the Biot number.

4.2 THE BOUSSINESQ APPROXIMATION.

Most simulations of free convection envoke the Boussinesq approximation. This states that variations in density are only important in the body force term of the momentum equations. In all other instances density variations are to be neglected. This approximation is valid in many problems but it was felt that it may become inaccurate in crystal growth problems because of the possibility of large temperature and concentration gradients. In an effort to study this a simulation was prepared using a modified Germanium-Silicon charge. The modifications included increasing the thermal expansion coefficient such that a maximum density difference of 10% was possible when a 300 C^0 temperature was impressed between the heater and the planar interface. Additionally, the concentration expansion coefficient was set equal to zero. The system properties are given in Table 2.

Specific heat	0.39 J/gm^0C
Gravity	980 cm/s^2
Thermal conductivity	0.51 W/cm^0C
Length of adiabatic zone	0.5 cm
Length of melt	2.0 cm
Radius of melt	0.5 cm
Thermal expansion coefficient	$3.33(10)^{-4}/^0C$
Concentration expansion coefficient	0
Kinematic viscosity	$1.3(10^{-3})cm^2/s$
Density	5.5 gm/cm^3
Temperature difference	300 C^0
Prandtl number	0.005
Grashof number(length)	$4.6(10^8)$

Table 2. Modified Germanium-Silicon System Properties

The results are rather startling. A maximum velocity of 6.49 cm/s was achieved in the steady state case using the Boussinesq approximation. This is in contrast to a maximum velocity of 5.34

cm/s when the exact equations are used. This difference of course has a tremendous effect on the transport process because the flow is recirculating and the error accumulates. Of particular interest is the heat transfer at the interface. As was shown in section 4.1 the shape of the interface plays a major role in determining the qualitative nature of the fluid flow. This shape is a function of the interfacial heat transfer. Figure 17 is a plot of Boussinesq to exact heat flux ratio versus radial distance along the interface. The liquid region was kept the same in both cases. The heat flux ratio varies between 14% and 36% across the interface. This is a large amount and certainly enough to change its shape from convex to concave if allowed. The lesson of this section is that the often used Boussinesq approximation is not valid in many cases of interest to crystal growers.

4.3 TRANSIENT THERMAL CONVECTION

A new code is currently being developed which accounts for the transient nature of the flow which may occur in practice. A sample case is included which uses the same modified Germanium-Silicon charge mentioned in the previous section. The boundary conditions are shown in figure 18. The initial condition is taken to be the steady state field which would be present if gravity were set equal to zero. This amounts to a conduction thermal field with fluid velocity everywhere zero. The interface in this case is essentially flat because the adiabatic zone is so long. Since the case is only being used to demonstrate the capability of the code the interface is made to remain stationary in order to minimize computer time. Actually it would move as convection altered the temperature field.

A time sequence of streamlines is presented in figure 19. The initially motionless melt starts moving and is characterized by a single cell which commences in the vicinity of the wall-interface junction and preceeds upward along the wall as time increases. This is shown in figures 19a and 19b. Its intensity increases dramatically until a second counter rotating cell, starting in the same area as the first, forms as in figure 19c. The second cell proceeds to get larger and also moves up the ampoule wall as seen in the sequence of figures 19d through 19f. The upper cell slowly diminishes in strength but is always much stronger than the second cell.

Figures 19g through 19i show the second cell spreading radially across the ampoule and a third cell forming in the vicinity of the interface. This third cell rotates in the same direction as the first but opposite to the second. The strength of the cells, i.e., the velocity, is greatest in the upper cell and diminishes as the interface is approached. This is so because the radial temperature gradients are greatest in the upper cell region.

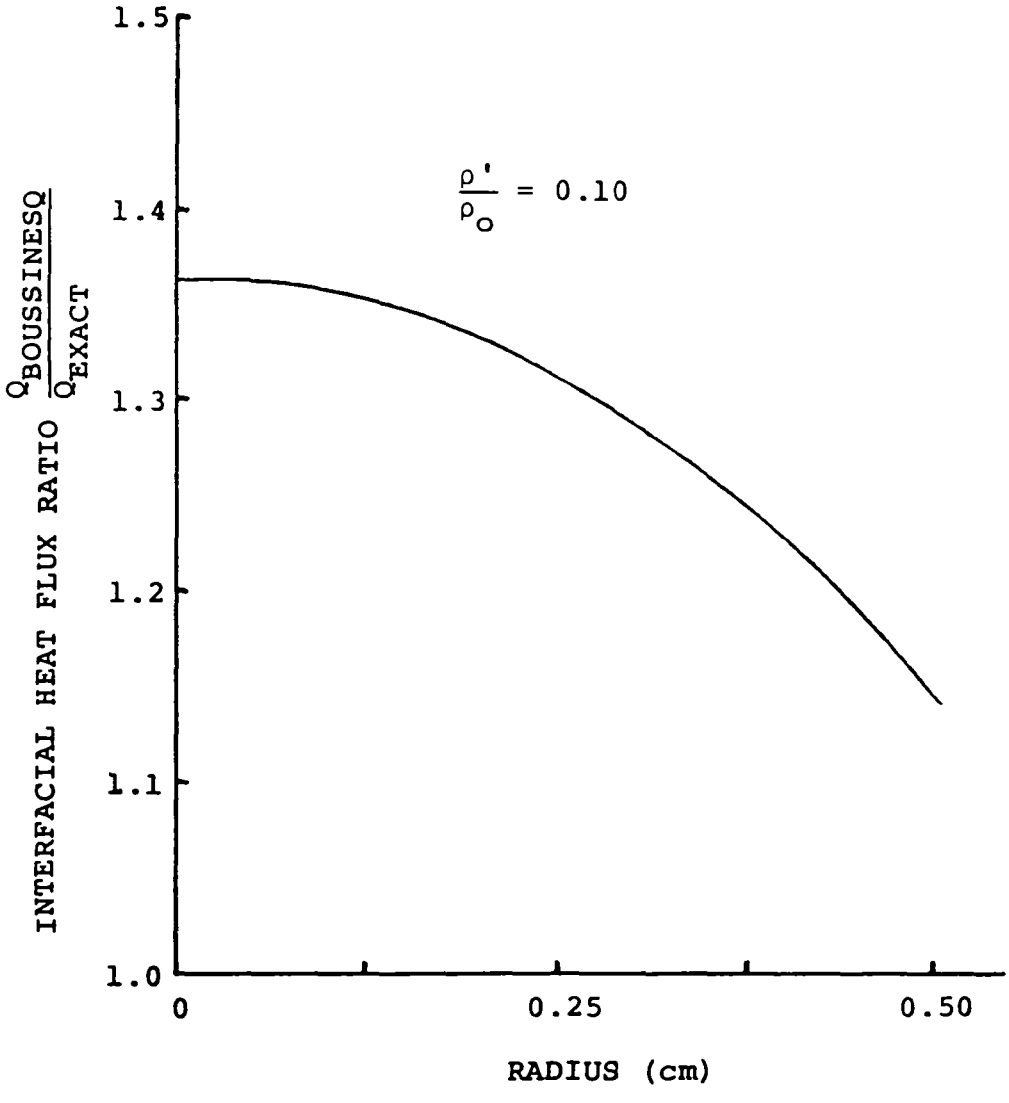

Figure 17. Interfacial heat flux ratio versus radius for $\rho'/\rho_0 = 0.1$.

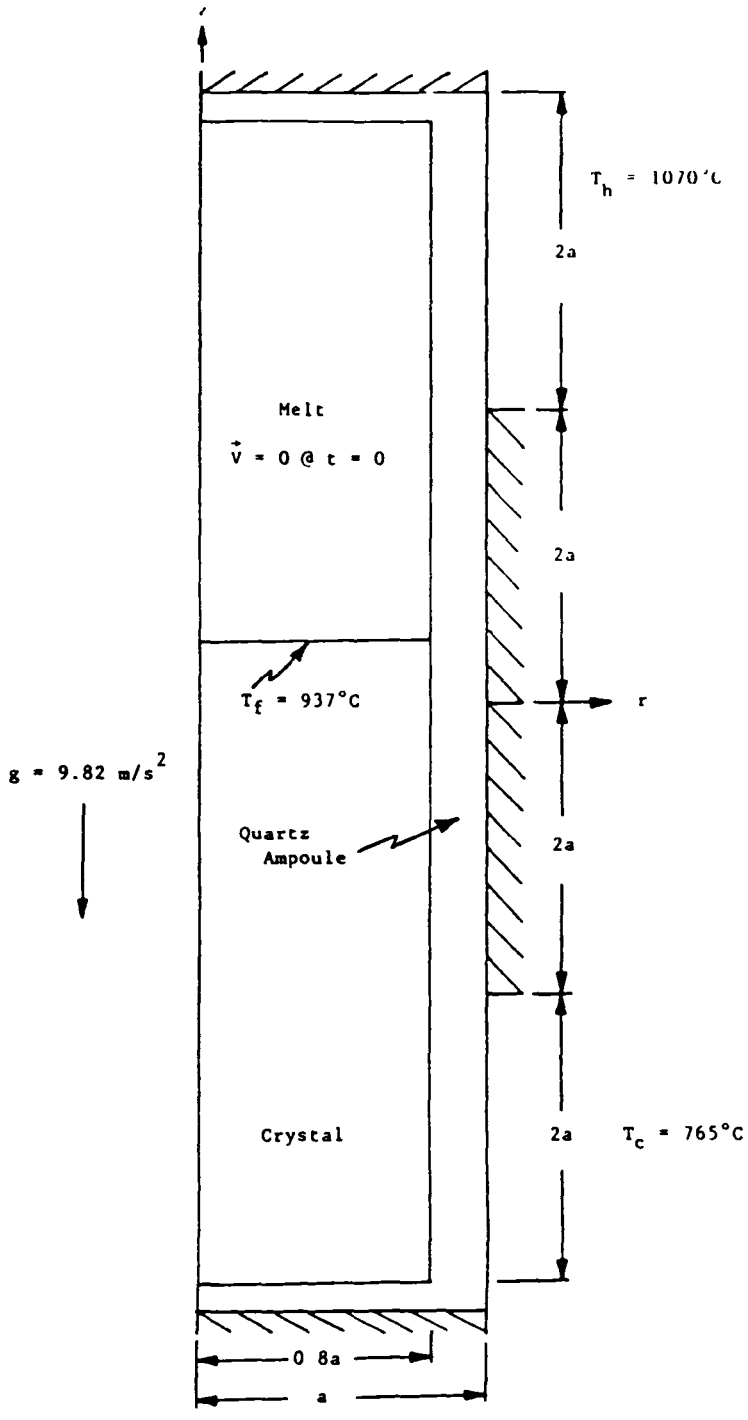

Figure 18. Initial condition of a stationary Gremanium-Silicon charge with a conduction temperature field.

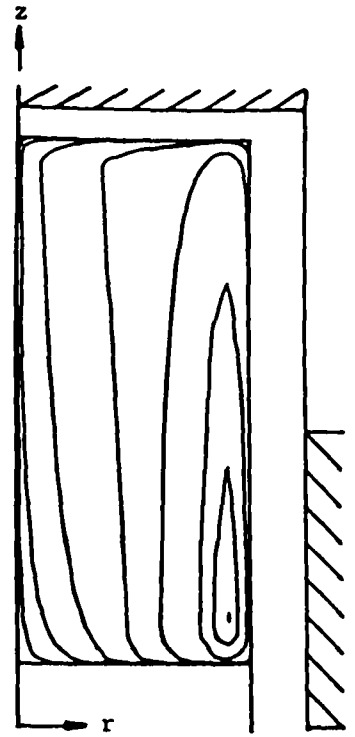

ψ_{max}=0.650E-08 m^3/s

ψ_{min}=0.0

ψ=0.65E-08
0.45E-08
0.20E-08
0.20E-09
0.20E-10
0.20E-11
0.20E-12
0.20E-13

time=0.04s

a

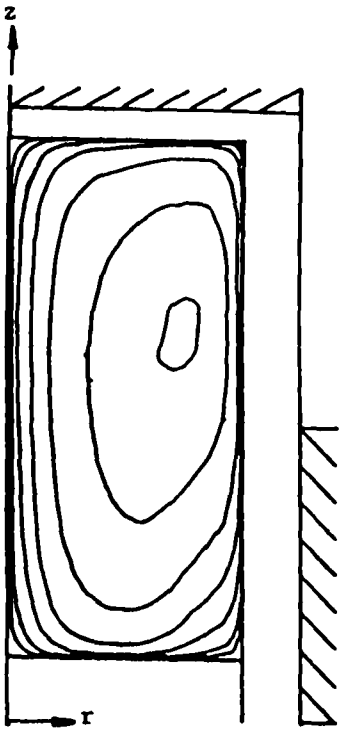

ψ_{max}=0.113E-08 m^3/s

ψ_{min}=0.0

ψ=0.11E-05
0.60E-06
0.20E-06
0.60E-07
0.20E-08
0.60E-08
0.20E-08

time=0.48s

b

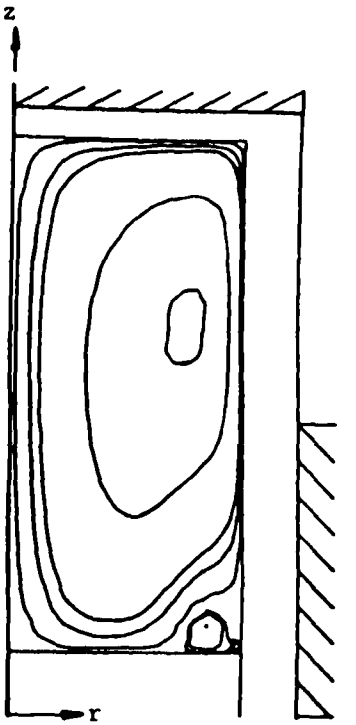

ψ_{max}=0.105E-05 m^3/s

ψ_{min}=-0.421E-08

ψ=0.10E-05
0.50E-06
0.10E-06
0.50E-07
0.10E-07
-0.42E-08
-0.10E-08
-0.10E-09
-0.50E-10
-0.10E-10

time=0.52s

c

Figure 18 a,b,c. Streamlines.

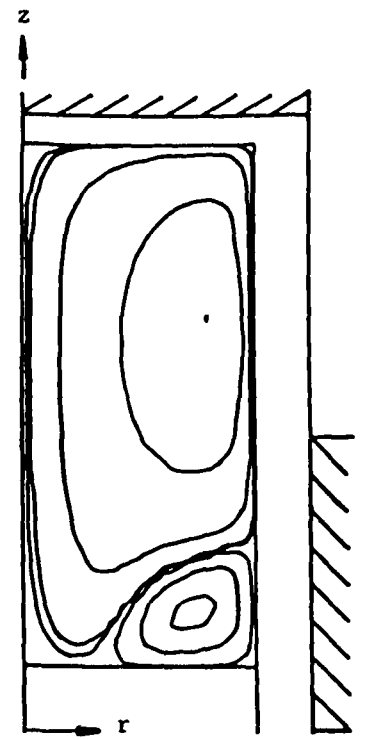

ψ_{max}=0.873E-06

ψ_{min}=-0.894E-07

ψ=0.87E-06
0.40E-06
0.80E-07
0.80E-08
0.40E-08
-0.80E-07
-0.40E-07
-0.80E-08

time=0.60s

d

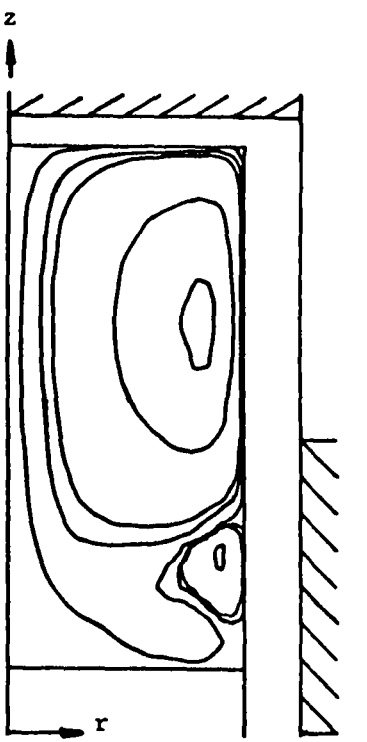

ψ_{max}=0.658E-06

ψ_{min}=-0.342E-07

ψ=0.60E-06
0.30E-06
0.60E-07
0.30E-07
0.60E-08
-0.30E-07
-0.30E-08
-0.30E-09

time=0.88s

e

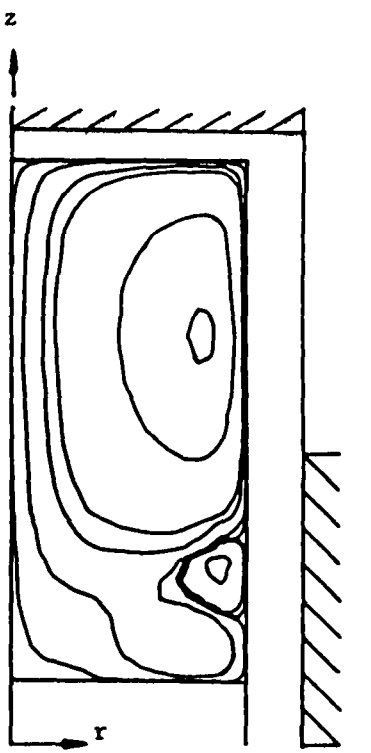

ψ_{max}=0.633E-06

ψ_{min}=-0.274E-07

ψ=0.60E-06
0.30E-06
0.60E-07
0.30E-07
0.60E-08
0.60E-09
-0.20E-07
-0.20E-08
-0.20E-09

time=0.90s

f

Figure 18 d,e,f. Streamlines.

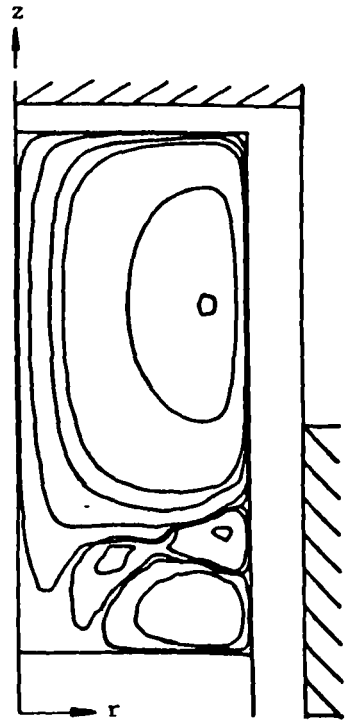

ψ_{max}=0.612E-06 m^3/s

ψ_{min}=-0.243E-07

ψ=0.60E-06
0.30E-06
0.60E-07
0.30E-07
0.60E-08
0.60E-09
-0.20E-07
-0.20E-08
-0.20E-09

time=0.92s

g

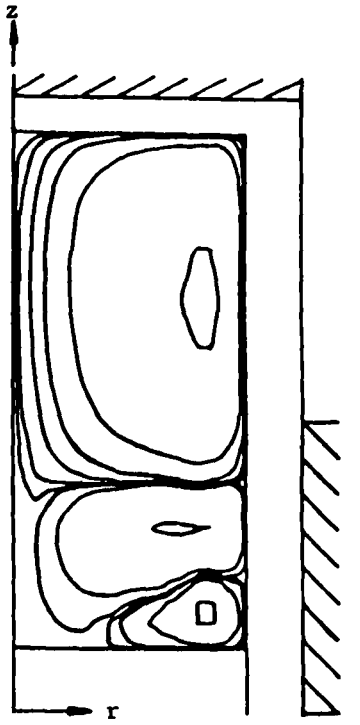

ψ_{max}=0.564E-06 m^3/s

ψ_{min}=-0.546E-07

ψ=0.50E-06
0.70E-07
0.20E-07
0.70E-08
0.20E-08
0.70E-09
-0.50E-07
-0.50E-08
-0.50E-09

time=1.00s

h

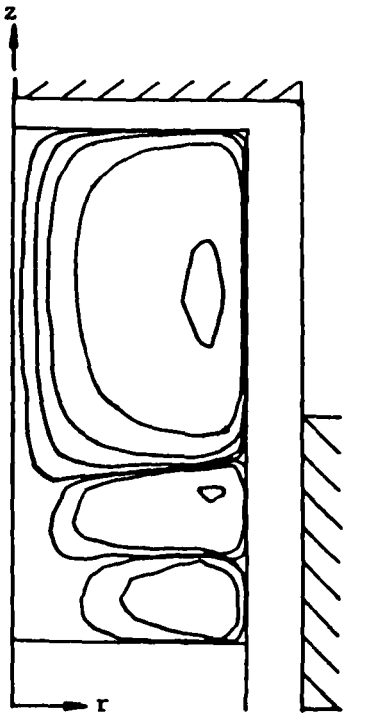

ψ_{max}=0.467E-06

ψ_{min}=-0.437E-07

ψ=0.40E-06
0.70E-07
0.20E-07
0.70E-08
0.20E-08
-0.40E-07
-0.40E-08
-0.40E-09

time=1.48s

i

Figure 18 g,h,i. Streamlines.

The flow appears to become steady and similar to figure 19i as time progresses. The calculation was terminated accordingly. As Grashof number increases multiple cells form. This is in contrast to the single cells of section 4.1. The current Grashof numbers are representative of those to be found in earth based processing. The proceeding calculations clearly show typical velocities and time scales to be expected in high Grashof number flows.

5.0 SUMMARY

It has been shown that it is important and possible to control the shape and position of the interface. Results were presented which theoretically proved this for diffusion dominated mass transfer. Experimentalists know this is true in the general case. A transient code was developed which is capable of predicting the fluid mechanics and heat transfer for growth conditions in both space and earth based systems. However, there are areas where the model needs improvement and more testing.

Future avenues of research should address the strong radiation heat transfer between the furnace and the ampoule including the ''adiabatic'' zone. Moreover, the finite ampoule thickness must be included in all heat transfer modelling. Moving the ampoule will produce fully time dependent conditions in which thermosolutal convection will predominate. This will necessitate the incorporation of a phase diagram into the code. These are difficult problems but not insurmountable.

6.0 REFERENCES

[1] L.Y. Chin, F.M. Carlson, J. Crystal Growth 62 (1983) p. 561.

[2] F.M. Carlson, L.Y. Chin, A.L. Fripp, R.K. Crouch, in Materials Processing in the Reduced Gravity Environment of Space, Ed. G.E. Rindone (North-Holland, New York, 1982) p. 629.

[3] F.M. Carlson, A.L. Fripp, R.K. Crouch, J. Crystal Growth 68 (1984) p. 747.

7.0 NOMENCLATURE

a	Radius of ampoule (m)
Bi	Biot number, ha/k
C, c	Species mass fraction
C_p	Specific heat (J/g.K)
D	Diffusion coefficient (m^2/s)
f	Interface position (m)
F	Dimensionless interface position, f/a
g	Gravitational acceleration (m/s^2)
Gr	Grashof number, $g\beta\Delta Ta^3(\rho/\mu)^2$
h	Heat transfer coefficient ($W/m^2.K$)
i	Insulation zone thickness (m)
I	Dimensionless insulation zone thickness, i/a
k	Thermal conductivity (W/m.K)
K	Segregation coefficient
l	Axial length (m)
L	Dimensionless length, l/a
n	Normal distance (m)
P, p	Pressure (N/m^2)
Pr	Prandtl number, $\mu C_p/k$
r	Radial coordinate (m)
R	Dimensionless radial coordinate, r/a
Sc	Schmidt number, $\mu/(\rho D)$
t	Temperature (K)
T	Dimensionless temperature
u	r or x velocity (m/s)
U	Dimensionless velocity, u/u_0
V_f	Interface velocity (m/s)
w	z or y velocity (m/s)
W	Dimensionless velocity, w/u_0
x	Cartesian coordinate (m)
y	Cartesian coordinate (m)
z	Axial coordinate (m)

Greek symbols

β	Thermal coefficient of volume expansion
γ	Growth rate, $2x_0V_f/D$
$\Delta()$	Denotes a change in ()
δ	Variable in Table 1.

η	Interface curvature index
μ	Molecular viscosity (kg/m.s)
ρ	Density (kg/m^3)
σ	Variable in Table 1.
τ	Time (s)
ϕ	Variable in Table 1.
ψ	Streamfunction (m^2/s)

Subscripts

c	Cool portion of furnace
f	Interface
h	Hot portion of furnace
l	Liquid (melt)
o	Reference (constant)
s	Solid (crystal)

End of Document